International Journal of Engineering

Journal Homepage: www.ije.ir

The Effect of Damping and Stiffness of Bearing on the Natural Frequencies of Rotor-bearing System

M. Eftekhari*

Department of Mechanical Engineering, Shahid Bahonar University of Kerman, Kerman, Iran

P A P E R I N F O

Paper history:
Received 31 October 2016
Received in revised form 24 November 2016
Accepted 09 February 2017

Keywords:
Rotor-bearing System
Bearing Stiffness
Bearing Damping
Campbell Diagram

A B S T R A C T

In this paper, the effectiveness of stiffness and damping of bearing is investigated on the natural frequencies of the rotor-bearing system. The rotor-bearing system consists of a shaft, two bearings and a disk between two bearings. Parallel spring-damper in horizental and vertical directions is considered for modeling the stiffness and damping of bearings. The gyroscopic effect is also considered in derivation of equations, together with its dependence on speed. Numerical results contain the critical speed of shaft for various values of bearing stiffness and damping. Moreover, the first six natural frequencies of rotor are presented in Campbell diagrams.

doi: *10.5829/idosi.ije.2017.30.03c.15*

1. INTRODUCTION

Rotor dynamics is the branch of engineering that studies the lateral and torsional vibrations of rotating shafts, with the objective of predicting the rotor vibrations and containing the vibration level under an acceptable limit [1]. Rotating machines are used for power transmission in modern engineering industries. Many industrial applications of rotors are generator, pump, compressor, gas turbine rotors installed in power plants and vehicle turbochargers. The dynamic behavior of rotors is changed by the mass unbalance and the support motions of rotor-bearing systems. In what follows, a review of the related works is presented.

Zorzi and Nelson investigated the instability of rotor-bearing system with internal and hysteric damping [2]. Lin and Lin studied the optimal weight design of rotor system [3]. Kang et al. studied the foundation effect on the dynamic characteristics of rotor-bearing systems [4]. Wu investigated the lateral vibration characteristics of the full-size rotor-bearing system using the scale rotor-bearing model [5]. Enemark and Santos applied the thermo-mechanical shape memory alloy springs in the rotor and bearing system [6]. Numerical results indicated that the vibration reductions up to around 50 percent can be achieved using the shape memory alloy springs (SMAs) instead of steel. Halminen et al. studied the dynamics of an active magnetic bearing-supported rotor during contact with a simulation model [7]. A new method combining the rational polynomials method (RPM) with the weighted instrumental variables (WIV) estimator was used to fit the directional frequency response function by Wang et al. [8]. In that work, the damping ratio of the first forward and backward modes were identified with high accuracy. Hao et al. [9] established a numerical model of the bending stiffness of the tapered roller bearing through mechanics and deformation analysis on the bearing-rotor system. Modal analysis on an air blower rotor system was carried out using transfer matrix method. Zhou et al. [10] presented the influence of stiffness and damping coefficients of the active magnetic bearings on the dynamic behavior of a rotor-bearing system. Jiang et al. [11] identified the equivalent stiffness and damping of AMB-rotor with multi-frequency excitation. The obtained results were in good agreement with the experimental results. Xu et al. [12] obtained the AMBs stiffness and damping coefficients for a rotor. The rotor was modeled as

*Corresponding Author's Email: *mojtaba.eftekhari59@gmail.com* (M. Eftekhari)

Please cite this article as: M. Eftekhari, The Effect of Damping and Stiffness of Bearing on the Natural Frequencies of Rotor-bearing System, International Journal of Engineering (IJE), TRANSACTIONS C: Aspects Vol. 30, No. 3, (March 2017) 448-455

Timoshenko beam and identification procedure based on the FE model. Xiang et al. [13] studied the dynamic behavior of a gear-bearing system with time varying stiffness. They reported that when the support stiffness was increased a diversity range of periodic and chaotic behaviors appeared. Wang et al. [14] defined the unbalance response of a rotor-bearing system as a function of position and the stiffness and damping coefficients of bearings. They proposed an analytical method to identify the rotor unbalance while operating. Modares Ahmadi et al. [15] investigated the dynamic response of a system of a flexible rotor and two ball bearings with squeeze film dampers and centralizing springs. Wang et al. [16] discussed the effects of axial preload, rotor eccentricity and inner/outer waviness amplitudes on the dynamic response of the rotor-bearing system.

In this paper, the vibration of the rolling bearing-rotor system is investigated. The supporting rolling element bearing is simplified as a particle on a shaft with parallel stiffness and damping elements in two directions (see Figure 1 (b)). Modal analysis of bearing-rotor system is carried out using the finite element method. The first six natural frequencies and critical speed are obtained for various values of bearing stiffness and damping.

2. GOVERNING EQATIONS

Figure 1 presents the scheme of a rotor. As shown in Figure 1(a), the components of rotor consist of a rotating shaft, two bearings b_1, b_2 and a disk with mass m and moment inertia J which is located at distance l_1 from b_1. As shown in Figure 1(a), the length of the undeformed shaft center line is l. A part of rotor's length (a in Figure 1(a)) is free for coupling to another shaft. Basic assumptions are: 1) the disk is rigid, 2) the shaft is deformable and modeled by Euler-Bernoulli beam of constant cross-section solicited in bending along two orthogonal directions, 3) the shaft and rigid disk are symmetric, 4) the bearings supporting the shaft are flexible and modeled as the spring-damper model as shown in Figure 1(b), 5) the spring-damper model of bearings are applied in x-y plane in x, y directions with spring coefficients k_x, k_y and damper coefficients c_x, c_y and 6) the rotor rotates at a constant speed Ω in z direction.

The equations of motion for the rigid disk, bearings and flexible shaft are derived by the use of Lagrange's theorem:

$$\frac{d}{dt}\left(\frac{\partial L}{\partial \dot{q}_i}\right) - \frac{\partial L}{\partial q_i} = F_i \quad (1)$$

where , in Equation (1), $L = T - U$ is the Lagrangian, T is the kinetic energy, U is the potential energy, q_i is the generalized coordinates describing the motion of the system and F_i is the generalized forces acting on the system. The symbol $\dot{()}$ refers to differentiation with respect to time. Generally, the equations of motion for the rotor system can be written as:

$$[M]\{\ddot{U}\} + [C]\{\dot{U}\} + [K]\{U\} = 0 \quad (2)$$

The system matrices of the equation of motion in Equation (2) are the global mass matrix $[M]$, the global damping matrix $[C]$ and the global stiffness matrix $[K]$. Moreover, $[U]$ is the global generalized displacement vector in x and y directions.

2. 1. Finite Element Analysis Modeling of the rotor-bearing system is performed by finite element method. Three elements are used for rotor-bearing problem. The elements are: BEAM188 element for the shaft, MASS 21 element for disk and COMBI 214 element for bearings.

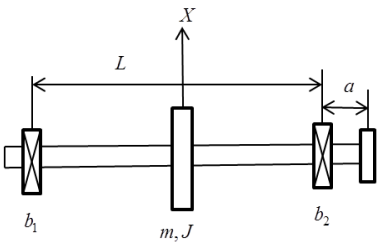

a) components of rotor model

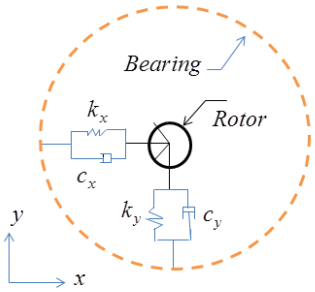

b) spring-damper model of bearing

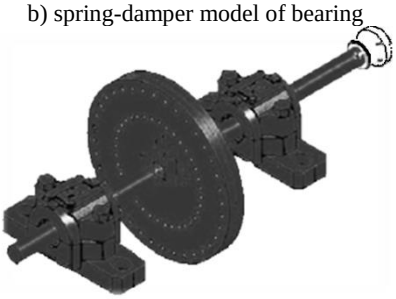

c) 3D model of rotor

Figure 1. Scheme of rotor model

The theory of BEAM188 element is based on the Timoshenko beam and the effect of shear deformation is evaluated in deflection of the element. The BEAM188 elemen consists of 6 degree of freedom. The MASS 21 element consists of 6 degree of freedom and has the different values of inertia in different directions. The COMBI 214 element contains of two node and each node has two degree of freedom. This element couples the stifness and damping in two directions (x and y direction).

3. RESULTS AND DISCUSSION

In this section, the effectiveness of parameters of rotor system is investigated in Campbell diagrams. The parameters are considered as: stiffness and damping of bearings (k_x, k_y, c_x, c_y), the location of symmetric disk (l_1), and the parameter a in Figure 1(a). Numerical results are divided into two cases: the effectiveness of stiffness and damping of bearing. The material characteristics and geometric properties of the rotor are listed in Table 1.

TABLE 1. Main characteristics of the on-board rotor

Density of shaft material	ρ_0=7800 kg/m^3	Young's modulus of the shaft	$E=200\times10^9$ N/m^2
Radius of the shaft	r_{shaft}=10 mm	Mass of the disk	4 kg
Length of the shaft	l= 200 mm	Moment of inertia of disk	$J=1.51\times10^{-2}$ kg.m^2
Location of disk	l_1= 100 mm		

The following non-dimensional parameters are defined in numerical results:

$$\overline{K}_x=\frac{K_xL^3}{EI},\ \overline{K}_y=\frac{K_yL^3}{EI},\ \zeta_x=\frac{c_x}{2\sqrt{K_xm}},\ \zeta_y=\frac{c_y}{2\sqrt{K_xm}}$$
$$\overline{\omega}_i=\frac{\omega_i}{\Omega_0},\ \overline{\Omega}=\frac{\Omega}{\Omega_0},\ \Omega_0=\sqrt{\frac{EI}{mL^3}}, \quad (3)$$

where, in Equation (3), $\overline{K}_x, \overline{K}_y$ are the non-dimensional stiffness of bearing in x and y directions, respectively, ζ_x, ζ_y are the non-dimensional damping of bearing in x and y directions, respectively, $\overline{\Omega}$ is the non-dimensional angular velocity of shaft and $\overline{\omega}_i$ is the ith non-dimensional natural frequency of shaft. Moreover, m is the mass of shaft and I is the second moment of area of shaft. In all figures, the angular velocity of shaft (Ω) is considered from 0 to 20000.

3. 1. The Effectiveness of Bearing Stiffness

Figure 2 presents the non-dimensional natural frequency (ω/Ω_0) versus the non-dimensional angular velocity of rotor (Ω/Ω_0) for three values of non-dimensional bearing stiffness. In order to verify and confirm the numerical results, the forward and backward natural frequencies are depicted for three values of bearing stiffness. The results are compared with the results presented in the literature [1] for a rotor with simply supported ends. As shown in Figure 2, when the bearing stiffness ($\overline{K}_x$) is increased from 0.1 to 1000, the natural frequencies are in good agreement with the simply supported rotor-shaft system.

Figure 3 shows the six natural frequencies of rotor-bearing system which are dependent on the shaft speed. In this figure, the non-dimensional natural frequencies are plotted versus the non-dimensional angular velocity of rotor. Figures 3(a)-3(f) show the six natural frequencies versus the angular velocity of rotor for $\zeta_x=\zeta_y=0$ and $\overline{K}_y/\overline{K}_x=1$. As shown in parts (a)-(f), as the value of Ω/Ω_0 increases, natural frequency is split into two frequencies (forward and backward) on account of the gyroscopic effect and the forward natural frequency increases and the backward natural frequency decreases. Also, for $\Omega/\Omega_0=0$, the forward and backward frequencies are the same. As the value of $\overline{K}_x$ is increased from 0.1 in Figure 3(a) to 1000 in Figure 3(f), the natural frequencies increase. Moreover, in parts (a)-(f) , the first and second natural frequencies (ω_1, ω_2) are coincide in whole considered interval of Ω/Ω_0. The gyroscope effect is not appeared in the first and second natural frequencies. As shown in Figures 3(a)-3(f), for larger values of bearing stiffness, the third, fourth, fifth and sixth natural frequencies are more far away.

In the other words, for a rotor-bearing system, when the damping of bearings is neglected and the stiffness of bearings is symmetric and increases, the forward natural frequencies increase and the backward natural frequencies decrease.

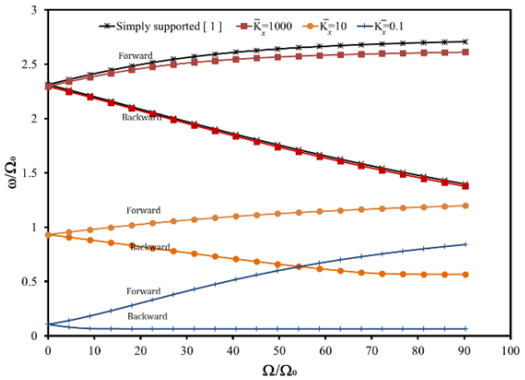

Figure 2. The non-dimensional natural frequency versus the non-dimensional angular velocity of rotor for three values of non-dimensional bearing stiffness $\overline{K}_x=0.1,10,1000$ $\zeta_x=\zeta_y=0,\ \overline{K}_y/\overline{K}_x=1$

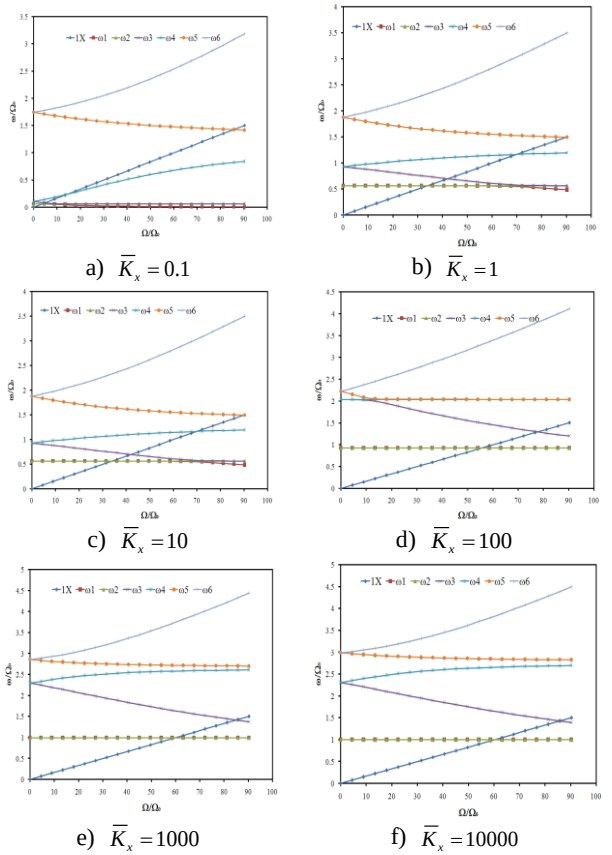

Figure 3. The non-dimensional natural frequencies versus the non-dimensional angular velocity for different values of bearing stiffness. $\zeta_x = \zeta_y = 0,\ \overline{K}_y / \overline{K}_x = 1.$

Moreover, by increasing the value of $\overline{K}_x$, the intersection of line 1X with the natural frequencies occurs at larger values of Ω/Ω_0.

The values of intersection ($\overline{\Omega}_i (i = 1,...,6)$) are presented in Table 2 for ith natural frequency. The dashed lines in Table 2 and all tables are the values of $\Omega \geq 20000\,(rpm)$. As seen in Table 2, the values of $\overline{\Omega}_1, \overline{\Omega}_2$ are close together, because the first and second natural frequencies are almost coincide with each other.

Figure 4 presents the non-dimensional natural frequency (ω/Ω_0) versus the non-dimensional bearing stiffness ($\overline{K}_x$) for $\Omega/\Omega_0 = 0$. As shown in Figure 4, when the gyroscope effect is ignored , by increasing the non-dimensional bearing stiffness the forward and backward frequencies are coincide together. For $\overline{K}_x > 1000$, the frequencies are almost unchanged and the frequencies are the values of rotor system with simply supported ends. Figure 4 shows that for a rotor-bearing system with symmetric bearing stiffness and without bearing damping, the forward and backward natural frequencies are same for any values of bearing stiffness at the shaft speed equal to zero.

Figure 5 presents the Campbell diagrams for various values of $\overline{K}_y / \overline{K}_x, \overline{K}_x = 15$ and $\zeta_x = \zeta_y = 0$. Natural frequencies are plotted versus the angular velocity of shaft. Figures 5(a)-(e) are shown for $0.1 \leq \overline{K}_y / \overline{K}_x \leq 2$. As shown in parts (a)-(e), when the Ω/Ω_0 increases the forward natural frequency increases and the backward natural frequency decreases. Figures 5(f) and 5(g) are for $\overline{K}_y / \overline{K}_x = 10,100$, respectively. As shown in parts (f) and (g), by increasing the Ω/Ω_0, the fifth mode increases and the fourth mode decreases. The intersection of line 1X with the natural frequencies is tabulated for different values of $\overline{K}_y / \overline{K}_x$ in parts (a)-(g) of Figure 5.

TABLE 2. The intersection values of line 1X with non-dimensional natural frequencies for $\zeta_x = \zeta_y = 0, \overline{K}_y / \overline{K}_x = 1$. (Non-dimensional angular velocity)

	$\overline{K}_x$ =0.1	$\overline{K}_x$ =1	$\overline{K}_x$ =10	$\overline{K}_x$ =100	$\overline{K}_x$ =1000	$\overline{K}_x$ =10000	$\overline{K}_x$ =100000
$\overline{\Omega}_1$	3.804949	11.9226	33.78101	55.44217	59.52998	59.95813	60.00109
$\overline{\Omega}_2$	3.856872	12.05007	33.82152	55.4422	59.55709	59.99418	60.03814
$\overline{\Omega}_3$	4.774073	14.83911	42.00901	77.83975	85.0458	85.79135	85.86715
$\overline{\Omega}_4$	14.42954	36.62045	70.06768	---	---	---	---
$\overline{\Omega}_5$	85.56061	85.93927	89.75627	---	---	---	---
$\overline{\Omega}_6$	---	---	---	---	---	---	---

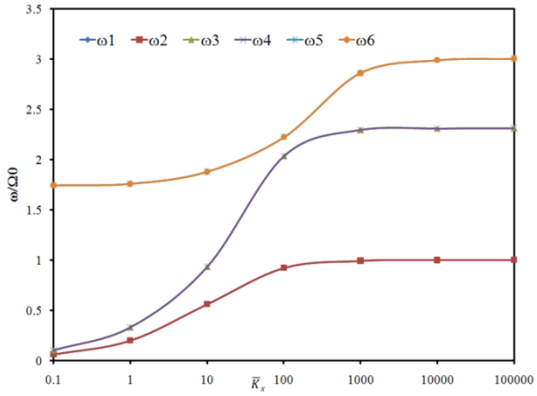

Figure 4. The non-dimensional natural frequencies versus the non-dimensional bearing stiffness for $\overline{\Omega}=0$, $\zeta_x=\zeta_y=0$, $\overline{K}_y/\overline{K}_x=1$.

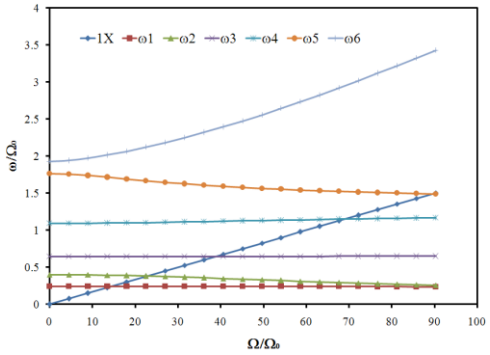

a) $\overline{K}_y/\overline{K}_x=0.1$

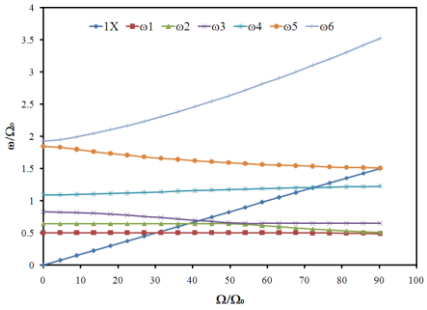

b) $\overline{K}_y/\overline{K}_x=0.5$

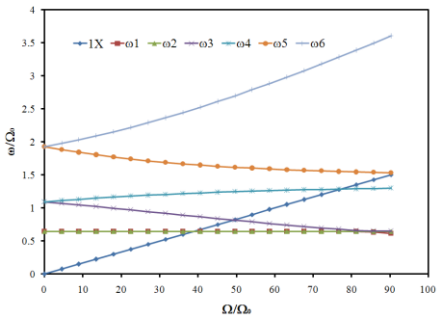

c) $\overline{K}_y/\overline{K}_x=1$

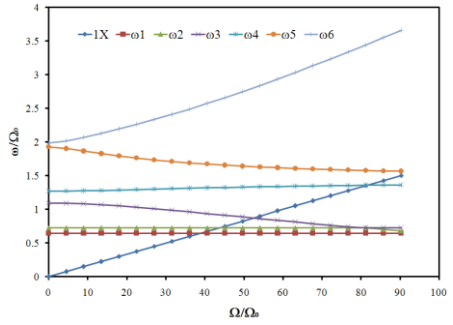

d) $\overline{K}_y/\overline{K}_x=1.5$

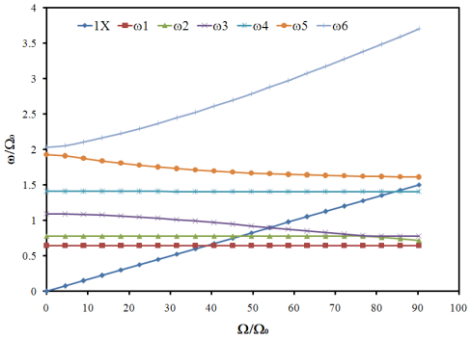

e) $\overline{K}_y/\overline{K}_x=2$

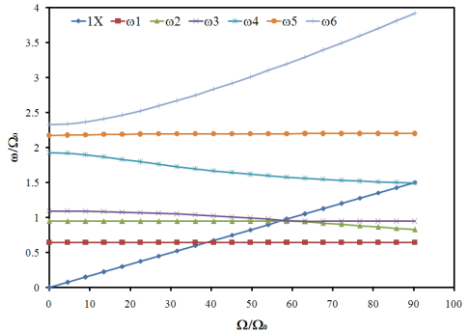

f) $\overline{K}_y/\overline{K}_x=10$

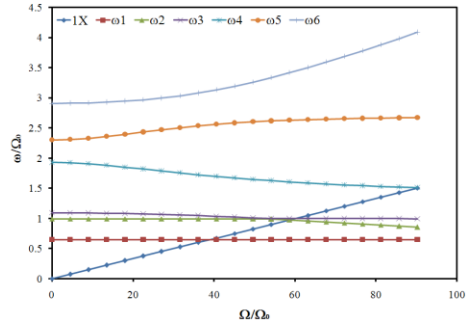

g) $\overline{K}_y/\overline{K}_x=100$

Figure 5. The non-dimensional natural frequencies versus the non-dimensional angular velocity for $\zeta_x=\zeta_y=0$, $\overline{K}_x=15$.

As seen in Table 3, as the value of $\overline{K}_y/\overline{K}_x$ increases, the critical speed occurs at higher values.

T ABLE 3. The intersection values of line 1X with non-dimensional natural frequencies for different values of $\overline{K}_y / \overline{K}_x$.

	$\overline{K}_y / \overline{K}_x$ =0.1	$\overline{K}_y / \overline{K}_x$ =0.5	$\overline{K}_y / \overline{K}_x$ =1	$\overline{K}_y / \overline{K}_x$ =1.5	$\overline{K}_y / \overline{K}_x$ =2	$\overline{K}_y / \overline{K}_x$ =10	$\overline{K}_y / \overline{K}_x$ =100
$\overline{\Omega}_1$	14.61925	30.22499	38.93382	38.93858	38.93883	38.93927	38.93935
$\overline{\Omega}_2$	22.93248	38.93056	38.94204	43.81949	46.92236	56.89875	58.56484
$\overline{\Omega}_3$	38.94222	41.68242	49.15931	52.37278	54.05189	57.91682	59.87676
$\overline{\Omega}_4$	69.03236	72.48293	77.30942	81.53168	84.44612	89.82579	---
$\overline{\Omega}_5$	89.51587	---	---	---	---	---	---

However, for $\overline{K}_y / \overline{K}_x \geq 1$, the value of $\overline{\Omega}_1$ is almost unchanged. Figure 6 shows the non-dimensional natural frequency versus the $\overline{K}_y / \overline{K}_x$ for $\Omega = 0$. As shown in Figure 6, for $\overline{K}_y / \overline{K}_x = 1$, the forward and backward frequencies are the same and for $\overline{K}_y / \overline{K}_x \neq 1$ the forward and backward frequencies are contrary. Moreover, for $\overline{K}_y / \overline{K}_x < 1$ the second and fourth frequencies are independent from $\overline{K}_y / \overline{K}_x$ and for $\overline{K}_y / \overline{K}_x > 1$ the first and third frequencies are independent from $\overline{K}_y / \overline{K}_x$.

3. 2. The Effectiveness of Damping Figure 7 shows the non-dimensional natural frequency (ω / Ω_0) versus the non-dimensional angular velocity of rotor (Ω / Ω_0) for different values of non-dimensional bearing damping. As shown in Figure 7, the first and second natural frequencies are independent from ζ. By increasing the bearing damping, the natural frequencies of higher modes decrease and the value of reduction is more in higher values of damping. Figure 7(d) presents that for $\zeta = 0.6$ the first, second, third and fourth natural frequencies are almost constant after the $\Omega / \Omega_0 > 40$.

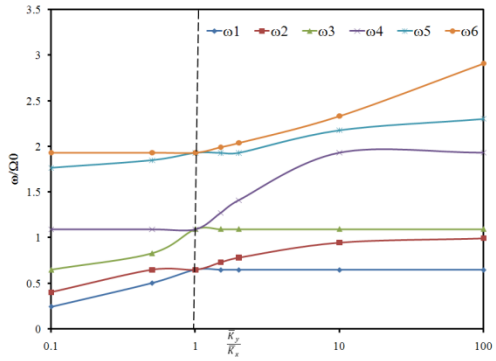

Figure 6. The non-dimensional natural frequency versus the $\overline{K}_y / \overline{K}_x$ for $\overline{\Omega} = 0$ $\zeta_x = \zeta_y = 0, \overline{K}_x = 15$.

Moreover, for low values of Ω / Ω_0 and high values of bearing damping, the natural frequencies of higher modes are lower than the first and second natural frequencies. It is noted from Figure 7 that for a rotor-bearing system, when the stiffness and damping of bearings are symmetric, the first and second natural frequencies are independent from damping in whole range of the angular velocity of rotor.

Figure 8 shows the non-dimensional natural frequencies versus the non-dimensional damping of bearing, when the effect of gyroscope effect is neglected. The first and second natural frequencies are independent from non-dimensional bearing damping. Rate of reduction of natural frequencies in third and fourth modes are more than fifth and sixth modes.

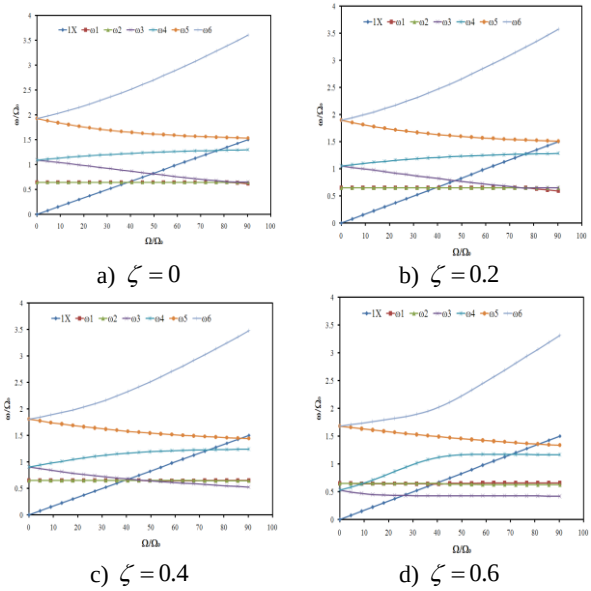

Figure 7. The non-dimensional natural frequencies versus the non-dimensional angular velocity for $\overline{K}_y / \overline{K}_x = 1$, $\zeta_x = \zeta_y = \zeta$, $\overline{K}_x = 15$, $\overline{\Omega} = 0$.

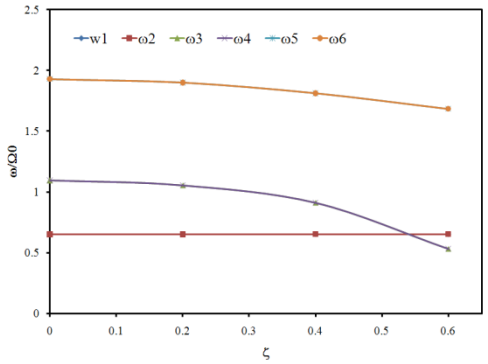

Figure 8. The non-dimensional natural frequency versus the non-dimensional damping for $\overline{K}_y/\overline{K}_x=1$, $\zeta_x=\zeta_y=\zeta$, $\overline{K}_x=15,\ \overline{\Omega}=0.$

The intersection of line 1X with the natural frequencies is tabulated for different values of ζ in parts (a)-(d) of Figure 7. As seen in Table 4, as ζ increases $\overline{\Omega}_1,\overline{\Omega}_2$ increase and $\overline{\Omega}_i, i\geq 3$ decrease.

TABLE 4. The intersection values of line 1X with non-dimensional natural frequencies for different values of $\zeta_x=\zeta_y=\zeta$ and $\overline{K}_y/\overline{K}_x=1,\overline{K}_x=15.$

	$\zeta=0$	$\zeta=0.2$	$\zeta=0.4$	$\zeta=0.6$
$\overline{\Omega}_1$	38.93383	38.97353	38.98611	38.46529
$\overline{\Omega}_2$	38.94204	38.98315	39.08322	39.31727
$\overline{\Omega}_3$	49.15932	47.23167	40.78638	26.11648
$\overline{\Omega}_4$	77.30943	76.40595	73.81131	70.38601
$\overline{\Omega}_5$	---	---	87.04071	81.5892

4. CONCLUDING REMARKS

The vibration analysis of a rotor-bearing system is studied for stiffness of bearing and angular velocity of shaft. The supporting bearing is modeled as a parallel spring-damper in x and y directions ($\overline{K}_x,\zeta_x,\overline{K}_y,\zeta_y$). The following results are obtained:

- By increasing the angular velocity of shaft and the bearing stiffness for $K_x=K_y,\zeta_x=\zeta_y=0$, the forward natural frequency increases and the backward frequency decreases. Moreover, the gyroscope effect is appeared in third, fourth, fifth and sixth natural frequencies. The critical speed of shaft occurs at higher values of bearing stiffness.
- By increasing the bearing stiffness ratio for $\overline{K}_x\neq\overline{K}_y,\zeta_x=\zeta_y=0$ the critical speed of shaft occurs at higher values and for $\overline{K}_y/\overline{K}_x\geq 1$, the value of $\overline{\Omega}_1$ is almost constant.
- By increasing the bearing damping, the first and second natural frequencies are almost independent from damping and the natural frequencies of higher modes decrease. Rate of reduction of natural frequencies in higher values of damping is more than the lower values.
- By increasing the damping of bearing, the first and second critical speeds of shaft increase and the third, fourth, fifth and sixth critical speeds of shaft decrease.

5. REFERENCES

1. Muszynska, A., "Rotordynamics, CRC press, (2005).
2. Nelson, H., "Finite element simulation of rotor-bearing systems with internal damping", ***Journal of Engineering for Power JANUARY***, (1977), 62-71.
3. Lin, Y.-H. and Lin, S.-C., "Optimal weight design of rotor systems with oil-film bearings subjected to frequency constraints", ***Finite Elements in Analysis and Design***, Vol. 37, No. 10, (2001), 777-798.
4. Kang, Y., Chang, Y.-P., Tsai, J.-W., Mu, L.-H. and Chang, Y.-F., "An investigation in stiffness effects on dynamics of rotor-bearing-foundation systems", ***Journal of sound and vibration***, Vol. 231, No. 2, (2000), 343-374.
5. Wu, J.-J., "Prediction of lateral vibration characteristics of a full-size rotor-bearing system by using those of its scale models", ***Finite Elements in Analysis and Design***, Vol. 43, No. 10, (2007), 803-816.
6. Enemark, S. and Santos, I.F., "Rotor–bearing system integrated with shape memory alloy springs for ensuring adaptable dynamics and damping enhancement—theory and experiment", ***Journal of Sound and Vibration***, Vol. 369, (2016), 29-49.
7. Halminen, O., Karkkainen, A., Sopanen, J. and Mikkola, A., "Active magnetic bearing-supported rotor with misaligned cageless backup bearings: A dropdown event simulation model", ***Mechanical Systems and Signal Processing***, Vol. 50, (2015), 692-705.
8. Wang, W., Li, Q., Gao, J., Yao, J. and Allaire, P., "An identification method for damping ratio in rotor systems", ***Mechanical Systems and Signal Processing***, Vol. 68, (2016), 536-554.
9. Wu, H., Zhou, Q., Zhang, Z. and An, Q., "Vibration analysis on the rolling element bearing-rotor system of an air blower", ***Journal of Mechanical Science and Technology***, Vol. 26, No. 3, (2012), 653-659.
10. Zhou, J., Di, L., Cheng, C., Xu, Y. and Lin, Z., "A rotor unbalance response based approach to the identification of the closed-loop stiffness and damping coefficients of active magnetic bearings", ***Mechanical Systems and Signal Processing***, Vol. 66, (2016), 665-678.
11. Jiang, K., Zhu, C., Chen, L. and Qiao, X., "Multi-dof rotor model based measurement of stiffness and damping for active magnetic bearing using multi-frequency excitation", ***Mechanical Systems and Signal Processing***, Vol. 60, (2015), 358-374.
12. Xu, Y., Zhou, J., Di, L. and Zhao, C., "Active magnetic bearings dynamic parameters identification from experimental rotor unbalance response", ***Mechanical Systems and Signal Processing***, Vol. 83, (2017), 228-240.

13. Xiang, L., Jia, Y. and Hu, A., "Bifurcation and chaos analysis for multi-freedom gear-bearing system with time-varying stiffness", ***Applied Mathematical Modelling***, Vol. 40, No. 23, (2016), 10506-10520.
14. Wang, A., Cheng, X., Meng, G., Xia, Y., Wo, L. and Wang, Z., "Dynamic analysis and numerical experiments for balancing of the continuous single-disc and single-span rotor-bearing system", ***Mechanical Systems and Signal Processing***, Vol. 86, (2017), 151-176.
15. Ahmadi, S.M., Ghazavi, M. and Sheikhzad, M., "Dynamic analysis of a rotor supported on ball bearings with waviness and centralizing springs and squeeze film dampers", ***International Journal of Engineering-Transactions C: Aspects***, Vol. 28, No. 9, (2015), 1351-1358.
16. Wang, H., Han, Q. and Zhou, D., "Nonlinear dynamic modeling of rotor system supported by angular contact ball bearings", ***Mechanical Systems and Signal Processing***, Vol. 85, (2017), 16-40.

The Effect of Damping and Stiffness of Bearing on the Natural Frequencies of Rotor-bearing System

M. Eftekhari

Department of Mechanical Engineering, Shahid Bahonar University of Kerman, Kerman, Iran

P A P E R I N F O

Paper history:
Received 31 October 2016
Received in revised form 24 November 2016
Accepted 09 February 2017

Keywords:
Rotor-bearing System
Bearing Stiffness
Bearing Damping
Campbell Diagram

چکیده

در این مقاله ، اثر فنریت و استهلاک یاتاقان بر روی فرکانسهای طبیعی سیستم روتور–یاتاقان بررسی می شود. سیستم روتور–یاتاقان شامل یک شافت ، دو یاتاقان و یک دیسک که در میان دو یاتاقان قرار دارد می باشد. مجموعه فنر – دمپر موازی در جهات افقی و عمودی برای مدل کردن فنریت و استهلاک یاتاقان ها در نظر گرفته می شود. اثر ژیروسکوپ در استخراج معادلات روتور در نظر گرفته می شود که وابسته به سرعت دورانی شافت می باشد. نتایج عددی شامل سرعت بحرانی شافت برای مقادیر مختلف فنریت و استهلاک یاتاقان می باشد. شش فرکانس طبیعی اول روتور در نمودارهای کمبل نشان داده می شود.

***doi**: 10.5829/idosi.ije.2017.30.03c.15*